EVALUATION OF DIFFERENT WORKING FLUID THERMODYNAMIC BEHAVIOR APPROACHES DURING CFD SIMULATIONS OF SINGLE PHASE EJECTORS

Vasileios Doulas[1], Nikolaos E. Karkalos[2], Antreas Nikoglou[2], Konstantinos Braimakis[1]*

[1]Laboratory of Refrigeration, Air-Conditioning & Solar Energy, School of Mechanical Engineering, National Technical University of Athens, Athens, Greece
[2]Laboratory of Thermal Processes, School of Mechanical Engineering, National Technical University of Athens, Athens, Greece

*Corresponding Author: nkark@mail.ntua.gr

Abstract:

The goal of the present work is to evaluate the impact of different thermodynamic modeling approaches on the numerical prediction of the operation and performance of a single-phase ejector using CFD simulations. The ejector is part of a trigeneration test facility integrating an Organic Rankine Cycle (ORC) with an ejector-based cooling system, operating with R1233zd(E) as working fluid, and is investigated over a range of operating conditions corresponding to different condensation pressures. Experimental measurements of pressure and temperature at the primary inlet, secondary inlet, and outlet are imposed as boundary conditions in the CFD model, while the predicted mass flow rates are validated against measurements obtained from flow meters. Four thermodynamic approaches are examined, including the ideal gas model, the Redlich–Kwong and Peng–Robinson equations of state, and polynomial correlations based on REFPROP data. The comparative assessment shows that, while all thermodynamic models predict the primary mass flow rate with relatively small differences, larger deviations are observed for the secondary flow rate and, consequently, for the entrainment ratio. Quantitatively, the entrainment-ratio deviations ranged from −11.82% to +10.86% for the polynomial model, −22.54% to −6.43% for Redlich–Kwong, −21.96% to -1.56% for Peng–Robinson, and −43.60% to −4.93% for the ideal gas model, confirming an overall agreement of the polynomial approach. In terms of computational cost, the ideal gas model was the least demanding, followed by the Redlich–Kwong and Peng–Robinson equations of state, while the polynomial correlations required higher solution times than the simplified models but remained considerably faster than direct REFPROP property calls.

1. INTRODUCTION

A supersonic ejector is a relatively simple device that operates by utilizing a high-pressure primary (motive) flow, which is accelerated through a converging–diverging nozzle. As the flow expands in the suction chamber, it entrains a low-pressure secondary flow. The two streams subsequently mix in the mixing section and are compressed in the diffuser. The operation of the ejector is governed by local fluid-dynamic phenomena(Besagni & Cristiani, 2021). The primary flow enters the nozzle at subsonic conditions, reaches sonic velocity at the throat, and is further accelerated to supersonic speeds in the diverging section, while its pressure continuously decreases. A detailed schematic of an ejector is shown in Fig. 1 (top).

At the bottom, the pressure and Mach number profiles of the ejector flow along different positions of the device are plotted(Braimakis, 2021).

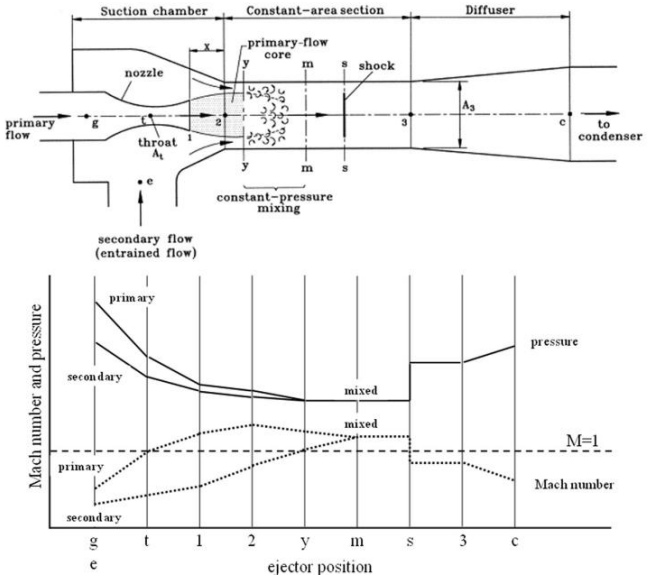

Figure 1: Ejector layout and pressure-Mach number profiles(Huang et al., 1999)

The operation of an ejector can be described through the relationship between entrainment ratio and backpressure, distinguishing three regimes. In the critical mode, both primary and secondary flows are choked, and the entrainment ratio reaches its maximum value, remaining independent of backpressure. As the backpressure increases beyond a critical value, the ejector enters the subcritical mode, where only the primary flow remains choked and the entrainment ratio decreases approximately linearly with further increases in backpressure. Finally, when the backpressure exceeds the critical backpressure, neither flow is choked and reverse flow occurs in the secondary stream, leading to negative entrainment ratios and malfunction of the ejector(Braimakis, 2021). The operation of ejectors of a given geometry is commonly expressed in the diagram shown in Fig. 2, which correlates the entrainment ratio with the ejector backpressure(Huang et al., 1999).

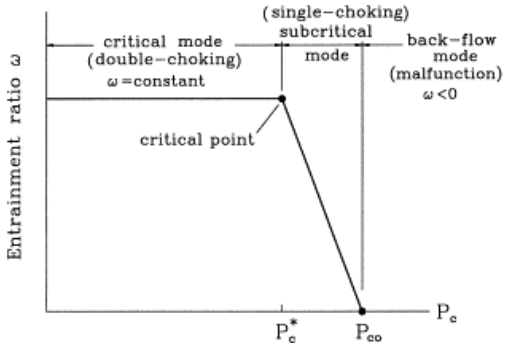

Figure 2: Entrainment ratio as a function of the ejector backpressure(Huang et al., 1999)

Ejectors are widely investigated as key components of ejector cooling cycles (ECC), which can serve as alternatives to conventional vapor compression systems, enabling the use of waste heat or solar thermal energy to generate cooling with minimal electrical energy consumption(Karkalos et al., 2024). Their main advantages include a simple and compact design, low operating and maintenance costs, and the absence of moving parts, resulting in long service life and minimal vibrations(Berghe et al., 2025; Yadav et al., 2021; Zhao & Ma, 2019), while their main drawback is their lower thermal coefficient of performance(Braimakis

et al., 2024).The precise estimation of ejector behavior, for different boundary conditions, is offundamental importance to determine system COP of analogous systems(Besagni & Cristiani, 2021). Nevertheless, hybrid ejector-based configurations have also been proposed in the literature, combining heat-driven ejector cooling with a mechanical compressor to increase operational flexibility (Braimakis & Karellas, 2024).

Theoretical analyses of ejectors commonly use one-dimensional (1-D) approaches, primarily employed for comparing different refrigerants and assessing system performance under varying operating conditions (Rusly et al., 2005). However, this approach becomes inadequate when detailed information about the flow field is required.1-D models may rely either on simplified numerical solutions of the governing 1-D flow equations (Berghe et al., 2025)or on analytical formulations based on the ideal gas law to describe fluid behavior within the ejector(Besagni et al., 2015; Park & Kang, 2023). Typical assumptions in such models include steady-state flow, constant thermophysical properties, ideal gas behavior, and the neglect of effects such as gravity, while often assuming isentropic processes.Alternatively, ejector modelling can be performed using computational fluid dynamics (CFD), which provides detailed insight into the flow field and thermophysical properties through numerical solution of the governing equations over the entire domain. Although more computationally demanding than 1-D approaches, CFD enables the simulation of complex phenomena such as heat transfer, radiation, and turbulence under various operating conditions and geometrical configurations, allowing for a more comprehensive analysis of flow behavior(Rusly et al., 2005).

Accurate thermophysical property modeling is essential in ejector CFD because it affects not only prediction accuracy, but also computational cost and convergence behavior. A suitable formulation should therefore reproduce real-fluid effects with sufficient accuracy, while avoiding excessive solution times and numerical instability. Although ideal-gas formulations have been widely used in supersonic ejector CFD studies due to their simplicity and low computational cost, mainly in works focused on turbulence modeling, geometry effects, and operating conditions, this assumption can become inaccurate for refrigerants under strongly compressible flow conditions (Bartosiewicz et al., 2006; Pianthong et al., 2007). Previous studies have shown that real-gas formulations, including REFPROP-based properties and cubic equations of state, can improve the prediction of entrainment ratio and internal shock-wave structures compared to the ideal-gas model, although often at the expense of increased computational cost and possible convergence difficulties(Croquer et al., 2016; Mazzelli & Milazzo, 2015). At the same time, the benefit of fully detailed real-gas simulations has been questioned in cases where the improvement in accuracy is limited compared to the additional computational effort(Vu & Kracik, 2018). In this context, the present work compares simplified and real-fluid thermodynamic models against experimental measurements obtained from a single-phase ejector operating with refrigerant R1233zd(E). In addition to conventional approaches, such as the ideal-gas model and cubic equations of state, polynomial thermophysical correlations fitted to high-accuracy REFPROP data are introduced, aiming to retain real-fluid accuracy while reducing computational cost and improving numerical robustness compared to direct REFPROP property evaluations. All approaches are validated under identical operating conditions using experimentally measured pressures, temperatures, and mass flow rates, allowing a direct assessment of their accuracy, computational performance, and suitability for ejector CFD simulations.

2. METHODOLOGY

2.1 Overview

The methodology followed in the present study aims at evaluating the impact of thermodynamic modeling approaches of R1233zd(E), on the prediction of ejector performance through CFD simulations, in direct comparison with experimental measurements. The ejector operation is investigated under experimentally measured boundary conditions, where the pressure and temperature values at the primary and

secondary inlets, as well as at the outlet, are imposed in the numerical model.A series of CFD simulations is performed using different thermodynamic property formulations, while maintaining identical geometry, mesh, and numerical setup, in order to isolate the effect of the thermodynamic model. The predictive capability of each approach is assessed by comparing the resulting mass flow rates of the primary and secondary streams with the corresponding experimental measurements obtained from flow meters.The entrainment ratio is used as the main performance indicator for the evaluation of the ejector operation. Through this procedure, the consistency between numerical predictions and experimental data is examined, allowing for a systematic assessment of the suitability of each thermodynamic modeling approach for ejector CFD simulations.

2.2 Ejector geometry

An ejector consists of three main sections: the converging–diverging nozzle (CDN), the constant-area section (CAS), and the diffuser(Karkalos et al., 2024). Their design is defined by several geometric parameters involving various cross-sectional flow areas, lengths, and angles, as shown in Fig. 3. In the present work, the ejector geometry was developed according to the design specifications of an ejector cooling cycle (ECC), which forms part of a hybrid Organic Rankine Cycle – Ejector Vapor Compression Cycle (EVCC) system for combined electricity, heating, and cooling production, utilizing waste heat, within the framework of the ZHENIT H2020 project(*ZHENIT H2020*, 2020).The geometry of the ejector considered in the present study, including its main geometric parameters, is illustrated in Fig.3 and Table 1.

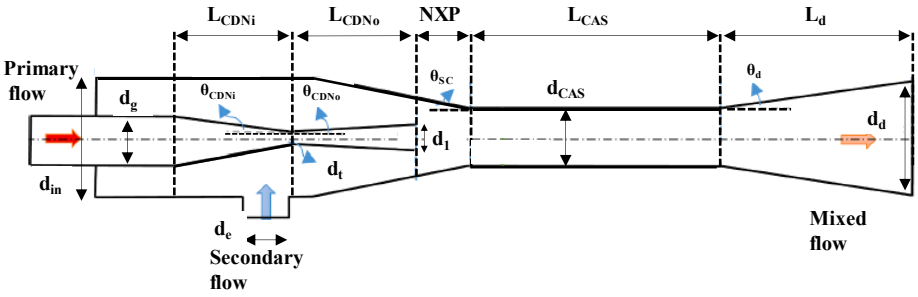

Figure 3: Ejector geometric parameters(Braimakis, 2021)

Table 1: Ejector main geometrical parameters

Converging-diverging nozzle dimensions	
d_g (mm)	8.00
d_e (mm)	16.92
d_t (mm)	2.90
d_1 (mm)	5.20
θ_{CDNi}(°)	12.00
θ_{CDNo}(°)	4.00
L_{CDNi}(mm)	11.99
L_{CDNo} (mm)	16.45
θ_{sc}(°)	30.00
NXP (mm)	16.80
d_{in} (mm)	27.99
Constant area section dimensions	
d_{CAS} (mm)	8.6
d_d (mm)	18.2
θ_d (°)	3.5

L_{CAS} (mm)	68.8
L_d(mm)	78.8

2.3 Description of CFD model

A computational model of the ejector was developed and simulated using the Finite Volume Method (FVM) in ANSYS Fluent software.The 3-D model of the ejector was developed based on the actual manufactured geometry, ensuring an accurate representation of the internal flow passages. The computational grid consisted of approximately 1259950 elements, with an average mesh quality of 0.74 and maximum quality close to unity (0.9999) ensuring a good balance between numerical accuracy and computational cost. In order to accurately capture near-wall gradients, 10 inflation layers were applied along the solid boundaries, enhancing the resolution of the boundary layer and improving the prediction of wall-bounded flow behavior.Lower-quality mesh elements are primarily observed in regions characterized by strong geometric gradients and boundary layer refinement near solid boundaries.

The governing equations of mass, momentum, and energy were solved under steady-state conditions.The simulations were performed using a pressure-based solver. Turbulence effects were modeled using the k-ω sstmodel(Besagni et al., 2021).

Convergence of the numerical solution was achieved when the residuals of the flow field were reduced below 10^{-5}, while additional monitoring of mass flow rates at the inlet and outlet ensured global mass conservation and solution stability.

Boundary conditions were defined directly from experimental measurements. Specifically, pressure and temperature values at the primary and secondary inlets, as well as at the outlet, were imposed in the simulations. This approach ensured consistency between the experimental setup and the numerical model, allowing for a direct comparison of the predicted and measured mass flow rates.

Finally, all simulations were performed using identical numerical settings, with variations only in the thermodynamic modeling approach. This ensured that any observed differences in the results could be attributed solely to the selected thermodynamic model.

2.4 Thermodynamic modeling approaches

The working fluid considered in the present study is R1233zd(E), which is widely used in ejector cooling and ORC applications due to its favorable thermophysical propertiesand environmental behavior (ultra low GWP and zero ODP). The critical properties and molecular weight of the fluid were considered$T_c = 165.6^oC$, $P_c = 36.23$ bar, $Mw = 130.5 kg/kmol$(Longo et al., 2020).Different thermodynamic models are compared to assess their impact on ejector performance, mainly through density prediction. The remaining properties are evaluated with polynomial correlations based on high-accuracy reference data.

The ideal gas model constitutes the simplest approach, where density is calculated as:

$$\rho = \frac{p}{RT} \tag{1}$$

The Redlich–Kwong equation of state is one of the earliest improvements over the classical van der Waals equation for the description of real-fluid behavior. It introduces a temperature-dependent attractive term, leading to a more accurate representation of gases at moderate temperatures and pressures(Soave, 1984).

The pressure is expressed as:

$$p = \frac{RT}{v-b} - \frac{a}{\sqrt{T}\, v(v+b)} \tag{2}$$

where $v$is the specific volume expressed as $v = \frac{1}{\rho}$.

The model parameters are defined as:

$$\mathrm{a} = 0.42748 \frac{\mathrm{R}^2 \mathrm{T}_\mathrm{c}^{2.5}}{\mathrm{P}_\mathrm{c}} \tag{3}$$

$$\mathrm{b} = 0.08664\frac{\mathrm{RT_c}}{\mathrm{P_c}} \tag{4}$$

In comparison to the van der Waals equation of state, where the attractive term is constant and independent of temperature:

$$p = \frac{RT}{v-b} - \frac{a}{v^2} \tag{5}$$

The Redlich–Kwong model introduces a temperature dependence of the form $T^{-0.5}$in the attractive term. Additionally, the denominator $v(v+b)$replaces the simpler v^2term of the van der Waals formulation(Soave, 1984).These modifications improve the prediction of thermodynamic properties, particularly at higher temperatures, where the van der Waals equation tends to overestimate intermolecular attractions.Despite this improvement, the Redlich–Kwong equation remains limited in accuracy near the critical region and under conditions approaching phase change, where more advanced equations of state, such as Peng–Robinson, provide better agreement with experimental data.

The Peng–Robinson equation of state represents a further development of cubic equations, providing improved accuracy in the prediction of thermodynamic properties, particularly for fluids near the critical region and for applications involving phase behavior(Mathias et al., 1989).
The pressure is expressed as:

$$p = \frac{RT}{v-b} - \frac{a}{v(v+b)+b(v-b)} \tag{6}$$

The model parameters are defined as:

$$a = 0.45724\frac{R^2T_c^2}{P_c}\alpha(T) \tag{7}$$

$$\mathrm{b} = 0.07780\frac{\mathrm{RT_c}}{\mathrm{P_c}} \tag{8}$$

$$\alpha(T) = \left[1 + \kappa\left(1 - \sqrt{\frac{T}{T_c}}\right)\right]^2 \tag{9}$$

$$\kappa = 0.37464 + 1.54226\omega_k - 0.26992{\omega_k}^2 \tag{10}$$

where $\omega_k$is the acentric factor of the fluid.

In contrast to the Redlich–Kwong equation, where the temperature dependence of the attractive term is limited to a simple $T^{-0.5}$relation, the Peng–Robinson model introduces a more flexible correction through the function $\alpha(T)$, which explicitly incorporates the acentric factor. This allows the equation to better capture deviations from ideal behavior and improves the prediction of fluid properties over a wider range of operating conditions(Mathias et al., 1989; Soave, 1984).

In the present study, the Peng–Robinson equation was implemented for the calculation of density, by solving the cubic equation for the specific volume and subsequently evaluating $\rho = \frac{1}{v}$.

In addition to analytical equations of state, a data-driven thermophysical property formulation was employed using polynomial correlations derived from REFPROP data. REFPROP is a thermodynamic software developed by NIST for the evaluation of thermophysical properties of pure fluids and mixtures using high-accuracy equations of state (Bell & Lemmon, 2016).

Although direct REFPROP coupling provides highly accurate property values, it increases the computational cost during CFD simulations due to repeated property evaluations throughout the iterative solution. Therefore, polynomial correlations were developed as a faster REFPROP-based alternative, reducing the solution time by approximately 50% while preserving property accuracy within the examined operating range. The required property data were generated over the pressure and temperature range corresponding to the gas-phase operating region of R1233zd(E), as defined from its pressure–enthalpy (P–h) diagram. To improve numerical stability and regression accuracy, normalized pressure and temperature variables were introduced:

$$p^* = \frac{p - p_{mean}}{\Delta \mathrm{p}} \tag{11}$$

$$T^* = \frac{T - T_{mean}}{\Delta T} \tag{12}$$

where $P_{mean}$and T_{mean} are the mean values of pressure and temperature, and ΔP, $\Delta T$are theirrespective ranges.

Each thermophysical property was then expressed as a polynomial function of the normalized variables:

$$\phi(P,T) = c_0 + c_1 p^* + c_2 T^* + c_3 p^* T^* + c_4 (p^*)^2 + c_5 (T^*)^2 + c_6 p^* (T^*)^2 + c_7 T^* (p^*)^2 + c_8 (T^*)^3 + c_9 (p^*)^3 \tag{13}$$

The polynomial fitting was applied to calculatedensity, specific heat capacity at constant pressure, dynamic viscosity, thermal conductivity and speed of sound. It should be noted that the specific heat capacity at constant pressurewas assumed to be a function of temperature only. The coefficients were obtained by minimizing the squared error between the polynomial prediction and the reference values obtained from REFPROP.

The accuracy of the polynomial approximation was evaluated using the mean absolute relative error:

$$\varepsilon = \frac{1}{N} \sum_{i=1}^{N} \left| \frac{\phi_{\mathrm{fit},i} - \phi_{\mathrm{ref},i}}{\phi_{\mathrm{ref},i}} \right| \times 100\% \tag{14}$$

Table 2 presents the mean absolute relative errors of the polynomial correlations, obtained using normalization factors of $P_{\mathrm{mean}} = 905000\mathrm{Pa}$, $\Delta P = 895000\mathrm{Pa}$, $T_{\mathrm{mean}} = 513.15\mathrm{K}$ and $\Delta T = 212\mathrm{K}$. This selection was made to ensure accurate prediction over the entire gas-phase range of R1233zd(E).

Table 2: Mean absolute relative error of polynomial correlations compared to REFPROP

Density(kg/m^3)	5.13%
Viscosity(Pa*s)	0.27%
Thermal conductivity(W/m*K)	0.58%
Speed of sound (m/s)	0.75%
Specific heat capacity(J/kg*K)	8.36%

These low error values indicate that the polynomial correlations provide an accurate representation of thermophysical properties within the investigated operating range. In the CFD simulations, the comparison between thermodynamic modeling approaches was primarily focused on the density calculation, obtained either from ideal gas assumptions, cubic equations of state, or polynomial correlations.

2.5 Experimental setup

The experimental investigation was conducted on a trigeneration test facility integrating an ORC with an ejector-based cooling system. The working fluid circulates through the ORC

loop, where it is evaporated subsequently and divided into two streams, with one expanding through the expander and the other directed to the ejector system.
Pressure, temperature, and mass flow rate were measured at the primary inlet, secondary inlet, and outlet of the ejector. These measurements were used both as boundary conditions in the CFD model and for validation of the predicted mass flow rates. During the experiments, the operating conditions at the evaporator were maintained constantly. The primary (motive) flow was supplied at a temperature of 70 °C and a pressure of 4.5 bar, while the secondary flow temperature was maintained at 17 °C. In contrast, the condenser conditions were varied by adjusting the temperature of the cooling medium in the condenser. This resulted in a controlled variation of the condensation temperature and, consequently, of the condensation pressure. As a result of this procedure, the ejector outlet conditions evolved according to the condenser operating conditions. The outlet temperature varied between 29 °C and 42 °C, corresponding to outlet pressures in the range of 1.3–2.1 bar. The corresponding pressure of the secondary flow was controlled by the constant opening of the secondary flow expansion valve.It is noted that the reported experimental values represent time-averaged measurements obtained under steady-state conditions.

3. RESULTS

The results obtained from the CFD simulationsand the experimental measurements are summarized in Tables 3–5. Specifically, Table 3 presents the primary mass flow rate, Table 4 the secondary mass flow rate, and Table 5 the corresponding entrainment ratio for all examined operating conditions and thermodynamic modeling approaches. For each case, the experimentally measured values are listed alongside the corresponding numerical predictions obtained using the polynomial correlations, the Redlich–Kwong equation of state, the Peng–Robinson equation of state, and the ideal gas model. The relative deviation of each model from the experimental measurements is also included in parentheses, providing a direct quantitative comparison between the different thermodynamic approaches.

Table 3: Primary mass flow for examined operating conditions and thermodynamic approaches

Condensation Pressure (bar)	Experimental $\dot{m}_p$(kg/s)	Polynomial $\dot{m}_p(kg/s)$	Redlich-Kwong $\dot{m}_p(kg/s)$	Peng-Robinson $\dot{m}_p(kg/s)$	Ideal gas $\dot{m}_p(kg/s)$
1.3	0.01373	0.0131 (-4.58%)	0.0128 (-6.72%)	0.0130 (-5.27%)	0.0125 (-8.89%)
1.5	0.01383	0.0131 (-5.27%)	0.0131 (-5.27%)	0.0131 (-5.27%)	0.0127 (-8.17%)
1.7	0.01343	0.0132 (-1.66%)	0.0131 (-2.38%)	0.0130 (-3.10%)	0.0127 (-5.27%)
1.9	0.01356	0.0132 (-2.6%)	0.0131 (-3.32%)	0.0131 (-3.32%)	0.0127 (-6.21%)
2.1	0.01325	0.0133 (+0.36%)	0.0131 (-1.08%)	0.0131 (-1.08%)	0.0127 (-3.97%)

Table 4: Secondary mass flow for examined operating conditions and thermodynamic approaches

Condensation Pressure (bar)	Experimental $\dot{m}_s$(kg/s)	Polynomial $\dot{m}_s(kg/s)$	Redlich-Kwong $\dot{m}_s(kg/s)$	Peng-Robinson $\dot{m}_s(kg/s)$	Ideal gas $\dot{m}_s(kg/s)$
1.3	0.0052	0.0052 (~0%)	0.0045 (-13.46%)	0.005 (-3.84%)	0.0045 (-13.46%)

1.5	0.0051	0.0052 (+1.92%)	0.0041 (-19.60%)	0.0043 (-15.68%)	0.0039 (-23.52%)
1.7	0.0045	0.0039 (-13.33%)	0.0034 (-24.44%)	0.0036 (-20%)	0.0024 (-46.66%)
1.9	0.0037	0.0032 (-13.51%)	0.0031 (-16.21%)	0.0028 (-24.32%)	0.0022 (-40.54%)
2.1	0.0025	0.0026 (+4%)	0.0022 (-12%)	0.0022 (-12%)	0.0017 (-32%)

Table 5: Entrainment ratio for examined operating conditions and thermodynamic approaches

Condensation Pressure (bar)	Experimental ω	Polynomial ω	Redlich-Kwong ω	Peng-Robinson ω	Ideal gas ω
1.3	0.378	0.419 (+10.86%)	0.354 (-6.43%)	0.384 (-1.56%)	0.360 (-4.93%)
1.5	0.368	0.396 (+7.64%)	0.312 (-15.12%)	0.328 (-10.57%)	0.312 (-15.39%)
1.7	0.335	0.295 (-11.82%)	0.259 (-22.54%)	0.279 (-16.71%)	0.188 (-43.60%)
1.9	0.272	0.242 (-11.15%)	0.236 (-13.27%)	0.213 (-21.96%)	0.173 (-36.51%)
2.1	0.188	0.195 (+3.6%)	0.167 (-10.99%)	0.167 (-10.92%)	0.133 (-29.05%)

Fig.4 presents the variation of the entrainment ratio as a function of the condensation pressure for the experimental measurements and all examined thermodynamic modeling approaches. As observed, theentrainment ratio decreases monotonically with increasing condensation pressure, indicating the progressive deterioration of ejector performance under higher backpressure conditions.

All models are able to reproduce the overall trend of the experimental data, although deviations become more pronounced at higher pressure levels. The polynomial model follows more closely the experimental curve throughout the entire range, while the remaining models show increasing divergence as the condensation pressure rises.

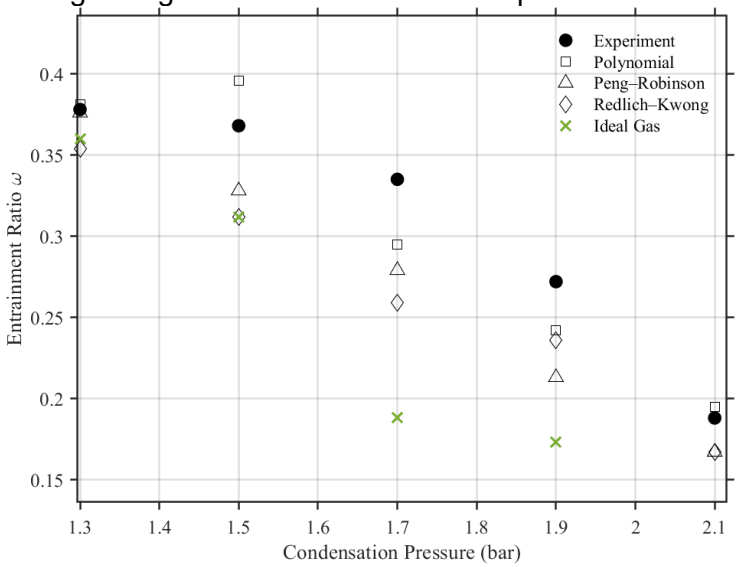

Figure 4: Entrainment ratio as a function of the condensation pressure for the experimental measurements and examined thermodynamic modeling approaches

Figs.5-7 present contour plots of velocity, pressure, and Mach number for a representative operating condition corresponding to a condensation pressure of 1.3 bar according to the simulations performed using the polynomial thermodynamic model.

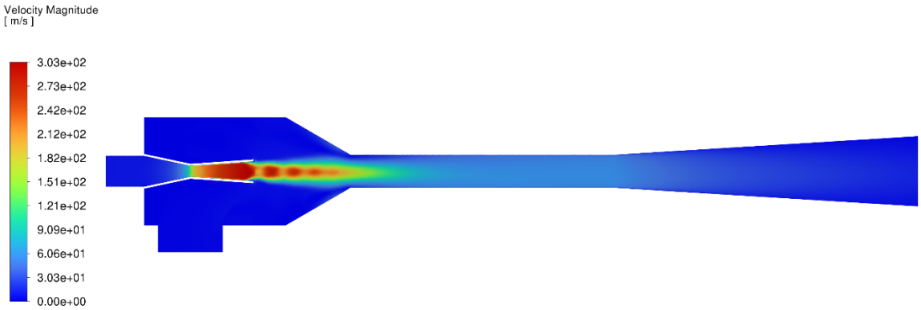

Figure 5: Velocity field

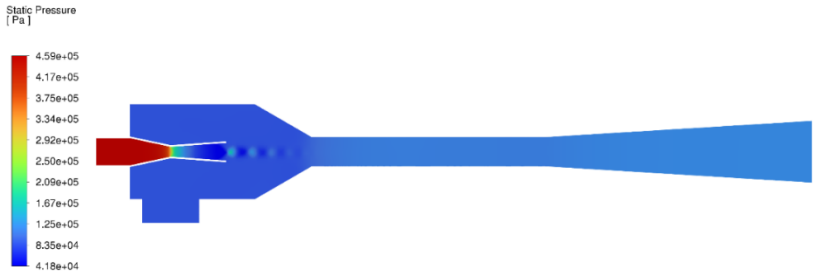

Figure 6: Static pressure field

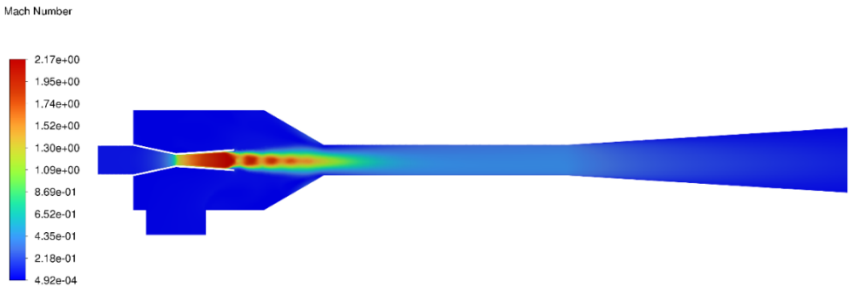

Figure 7: Mach number field

The velocity and Mach number contours (Figs. 5 and 7) indicate the acceleration of the primary flow in the nozzle, reaching sonic conditions (M = 1) at the throat and supersonic values downstream, followed by shock structures and gradual deceleration in the mixing section and diffuser. The pressure distribution (Fig. 6) shows a significant drop in the nozzle and a subsequent recovery along the diffuser.

4. CONCLUSION

The results show that the thermodynamic property model strongly affects the prediction of ejector performance, mainly through the secondary mass flow rate and the entrainment ratio, while the primary mass flow rate is predicted similarly by all models. The polynomial correlations provide the best agreement with the experimental data, since they are directly fitted to REFPROP properties. For the entrainment ratio, the deviations of the polynomial model range from −11.82% to +10.86%, giving the lowest overall error among the tested approaches. The Peng–Robinson and Redlich–Kwong equations of state show intermediate accuracy, with deviations ranging from −21.96% to −1.56% and from −22.54% to −6.43%,

respectively. Both models account for real-gas effects, but their simplified formulations lead to larger deviations than the polynomial approach. The ideal gas model gives the poorest predictions, with entrainment-ratio deviations from −43.60% to −4.93%, confirming that the ideal-gas assumption is not suitable for the present operating range. Overall, the CFD results mostly underpredict the secondary mass flow rate and, consequently, the entrainment ratio. Nevertheless, all models reproduce the experimentally observed decrease of entrainment ratio with increasing condensation pressure, showing that the numerical model captures the main performance trend.

NOMENCLATURE

Abbreviations

CAS	ejector Constant Area Section
CDN	Converging-diverging nozzle
CFD	Computational Fluid Dynamics
COP	Coefficient of Performance
ECC	Ejector Cooling Cycle
EVCC	Ejector-Vapor Compression Cycle
FVM	Finite Volumes Method
NXP	Nozzle Exit Position
WHR	Waste Heat Recovery

Greek characters

μ	dynamic viscosity	(Pa*s)
ρ	density	(kg/m^3)
ω	entrainment ratio	(-)
ω_k	acentric factor	(-)

Variables

c_p	specific heat capacity	(kJ/kg*K)
k	thermal conductivity	(W/m*K)
M	Mach number	(-)
$\dot{m}$	mass flow rate	(kg/s)
M_w	molecular weight	(kg/kmol)
p	pressure	(bar)
$\tilde{R}$	ratio of working fluid gas constant divided by global gas constant	(-)
T	temperature	(K)
v	Specific volume	(m^3/kg)

Subscripts

1	ejector CDN outlet
c	critical
CAS	constant area section of ejector
CDNi	converging-diverging nozzle inlet
CDNo	converging-diverging nozzle outlet
d	diffuser
e	ejector low-pressure port
g	ejector high-pressure port
in	inlet
mix	mixing
out	outlet
p	primary flow
s	secondary flow

t CDN throat
w weight (molecular)

REFERENCES

Bartosiewicz, Y., Aidoun, Z., & Mercadier, Y. (2006). Numerical assessment of ejector operation for refrigeration applications based on CFD. *Applied Thermal Engineering*, *26*(5–6), 604–612. https://doi.org/10.1016/j.applthermaleng.2005.07.003

Bell, I. H., & Lemmon, E. W. (2016). Automatic Fitting of Binary Interaction Parameters for Multi-fluid Helmholtz-Energy-Explicit Mixture Models. *Journal of Chemical & Engineering Data*, *61*(11), 3752–3760. https://doi.org/10.1021/acs.jced.6b00257

Berghe, J. V. den, Mendez, M. A., & Bartosiewicz, Y. (2025). *On the choking mechanism in supersonic ejectors: A one-dimensional analysis of Reynolds-Averaged Navier Stokes simulations* (arXiv:2510.23385). arXiv. https://doi.org/10.48550/arXiv.2510.23385

Besagni, G., & Cristiani, N. (2021). Multi-scale evaluation of an R290 variable geometry ejector. *Applied Thermal Engineering*, *188*, 116612. https://doi.org/10.1016/j.applthermaleng.2021.116612

Besagni, G., Cristiani, N., Croci, L., Guédon, G. R., & Inzoli, F. (2021). Computational fluid-dynamics modelling of supersonic ejectors: Screening of modelling approaches, comprehensive validation and assessment of ejector component efficiencies. *Applied Thermal Engineering*, *186*, 116431. https://doi.org/10.1016/j.applthermaleng.2020.116431

Besagni, G., Mereu, R., Di Leo, G., & Inzoli, F. (2015). A study of working fluids for heat driven ejector refrigeration using lumped parameter models. *International Journal of Refrigeration*, *58*, 154–171. https://doi.org/10.1016/j.ijrefrig.2015.06.015

Braimakis, K. (2021). Solar ejector cooling systems: A review. *Renewable Energy*, *164*, 566–602. https://doi.org/10.1016/j.renene.2020.09.079

Braimakis, K., Kalyvas, S., Palamidis, G., Roumpedakis, T., Charalampidis, A., Varvagiannis, E., & Karellas, S. (2024). DEVELOPMENT AND EXPERIMENTAL ASSESSMENT OF A SOLAR COOLING SYSTEM BASED ON EJECTOR COOLING CYCLE. *37th International Conference on Efficiency, Cost, Optimization, Simulation and Environmental Impact of Energy Systems (ECOS 2024)*, 1375–1386. https://doi.org/10.52202/077185-0118

Braimakis, K., & Karellas, S. (2024). Thermodynamic investigation of integrated organic Rankine cycle-ejector vapor compression cooling cycle waste heat recovery configurations for cooling, heating and power production. *Energy*, *304*, 132020. https://doi.org/10.1016/j.energy.2024.132020

Croquer, S., Poncet, S., & Aidoun, Z. (2016). Turbulence modeling of a single-phase R134a supersonic ejector. Part 1: Numerical benchmark. *International Journal of Refrigeration*, *61*, 140–152. https://doi.org/10.1016/j.ijrefrig.2015.07.030

Huang, B. J., Chang, J. M., Wang, C. P., & Petrenko, V. A. (1999). A 1-D analysis of ejector performance. *International Journal of Refrigeration*, *22*(5), 354–364. https://doi.org/10.1016/S0140-7007(99)00004-3

Karkalos, N., Braimakis, K., Markopoulos, A., Leontaritis, A.-D., & Karellas, S. (2024). COMPARISON OF 1-D EJECTOR MODELLING APPROACH AND COMPUTATIONAL FLUID DYNAMICS (CFD) SIMULATION TO PREDICT THE PERFORMANCE OF EJECTOR DEVICES. *37th International Conference on Efficiency, Cost, Optimization, Simulation and Environmental Impact of Energy Systems (ECOS 2024)*, 1936–1947. https://doi.org/10.52202/077185-0166

Longo, G. A., Mancin, S., Righetti, G., Zilio, C., & Steven Brown, J. (2020). Assessment of the low-GWP refrigerants R600a, R1234ze(Z) and R1233zd(E) for heat pump and organic Rankine cycle applications. *Applied Thermal Engineering*, *167*, 114804. https://doi.org/10.1016/j.applthermaleng.2019.114804

Mathias, P. M., Naheiri, T., & Oh, E. M. (1989). A density correction for the Peng—Robinson equation of state. *Fluid Phase Equilibria*, *47*(1), 77–87. https://doi.org/10.1016/0378-3812(89)80051-2

Mazzelli, F., & Milazzo, A. (2015). Performance analysis of a supersonic ejector cycle working with R245fa. *International Journal of Refrigeration*, *49*, 79–92. https://doi.org/10.1016/j.ijrefrig.2014.09.020

Park, H., & Kang, S. H. (2023). Development of a 1D solution algorithm to predict ejector performance in high altitude wind tunnels. *Journal of Mechanical Science and Technology*, *37*(11), 6037–6045. https://doi.org/10.1007/s12206-023-1042-0

Pianthong, K., Seehanam, W., Behnia, M., Sriveerakul, T., & Aphornratana, S. (2007). Investigation and improvement of ejector refrigeration system using computational fluid dynamics technique. *Energy Conversion and Management*, *48*(9), 2556–2564. https://doi.org/10.1016/j.enconman.2007.03.021

Rusly, E., Aye, L., Charters, W. W. S., & Ooi, A. (2005). CFD analysis of ejector in a combined ejector cooling system. *International Journal of Refrigeration*, *28*(7), 1092–1101. https://doi.org/10.1016/j.ijrefrig.2005.02.005

Soave, G. (1984). Improvement of the Van Der Waals equation of state. *Chemical Engineering Science*, *39*(2), 357–369. https://doi.org/10.1016/0009-2509(84)80034-2

Vu, N. V., & Kracik, J. (2018). CFD simulation of ejector: Is it worth to use real gas models? *EPJ Web of Conferences*, *180*, 02075. https://doi.org/10.1051/epjconf/201818002075

Yadav, S. K., Murari Pandey, K., & Gupta, R. (2021). Recent advances on principles of working of ejectors: A review. *Materials Today: Proceedings*, *45*, 6298–6305. https://doi.org/10.1016/j.matpr.2020.10.736

Zhao, X., & Ma, X. (Eds.). (2019). *Advanced Energy Efficiency Technologies for Solar Heating, Cooling and Power Generation*. Springer International Publishing. https://doi.org/10.1007/978-3-030-17283-1

ZHENIT H2020. (2020). ZHENIT H2020. https://www.zhenit.eu/